Flow, Turbulence and Combustion **60:** 105–122, 1998.

Investigation of Modeling for Non-Premixed Turbulent Combustion

S.M. DE BRUYN KOPS, J.J. RILEY and G. KOSÁLY
Department of Mechanical Engineering, University of Washington, Box 352600, Seattle, WA 98195-2600, U.S.A.

A.W. COOK
L-22, Lawrence Livermore National Laboratory, P.O. Box 808, Livermore, CA 94550, U.S.A.

Received 24 March 1998; accepted in revised form 25 September 1998

Abstract. A method for predicting filtered chemical species concentrations and filtered reaction rates in Large-Eddy Simulations of non-premixed, non-isothermal, turbulent reacting flows has been demonstrated to be quite accurate for higher Damköhler numbers. This subgrid-scale model is based on flamelet theory and uses presumed forms for both the dissipation rate and subgrid-scale probability density function of a conserved scalar. Inputs to the model are the chemistry rates, the Favre-filtered scalar, and its subgrid-scale variance and filtered dissipation rate. In this paper, models for the filtered dissipation rate and subgrid-scale variance are evaluated by filtering data from 512^3-point Direct Numerical Simulations of a single-step, isothermal reaction developing in the isotropic, incompressible, decaying turbulence field of Comte-Bellot and Corrsin. Both the subgrid-scale variance and the filtered dissipation rate models (the "sub-models") are found to be reasonably accurate. The effect of the errors introduced by the sub-models on the overall model is found to be small, and the overall model is shown to accurately predict the spatial average of the filtered species concentrations over a wide range of times.

Key words: large-eddy simulations, reacting flows, subgrid-scale models.

1. Introduction

Accounting for chemical reactions in a Large-Eddy Simulation (LES) requires knowledge of the distribution of reactants within each LES grid cell, and several approaches have been investigated by different researchers [2, 5, 13, 18, 23, 25, 38, 42]. One aspect of the strategy investigated in this paper for accounting for subgrid-scale mixing is the utilization of an assumed form for the Probability Density Function (PDF) of a conserved scalar within a grid volume. Gao and O'Brien [14] refer to this type of PDF as a Large-Eddy Probability Density Function (LEPDF). Bilger [1] and Lentini [21] found that errors in assumed PDF's are greatly reduced upon integration, a common operation which is required in order to obtain, e.g., average or filtered concentrations. Frankel et al. [12] and Cook and Riley [8] demonstrated the assumed LEPDF approach to be both practical and accurate for LES with equilibrium chemistry. In treating non-equilibrium chemistry,

Frankel et al. [12] employed a joint Beta distribution for the fuel and oxidizer in a flow with a single-step reaction. Specification of the joint LEPDF requires modeling the subgrid-scale species covariance, a quantity that is very difficult to obtain accurately. An alternative method of accounting for non-equilibrium chemistry is to invoke the quasi-steady version of the flamelet approximation of Peters [32]. This approach, combined with Reynolds Averaged Navier Stokes computations, has been recently applied to predict average species mass fractions in turbulent hydrogen-air flames [4, 33, 36]. The accurate predictions of data provide encouragement to apply the quasi-steady flamelet approach in the LES of turbulent combustion. To do so requires knowledge of the filtered dissipation rate and the subgrid-scale (SGS) variance of the scalar, quantities that potentially can be accurately modeled in an LES, since they are established by the large scales.

Cook et al. [10] used flamelet theory, in conjunction with an assumed LEPDF, to derive a model for the filtered chemical species in an incompressible, isothermal flow with a single-step reaction. The model was termed the Large-Eddy Laminar Flamelet Model (LELFM). Cook and Riley [9] extended the LELFM theory to the case of compressible flows with multi-step, Arrhenius-rate chemistry. *A priori* tests of the model using data from Direct Numerical Simulations (DNS) indicated that the LELFM is accurate, and improves with increasing Damköhler number. In the research reported in those papers, both the scalar subgrid-scale variance and filtered dissipation rate were computed directly by filtering data from the DNS.

The purpose of this paper is twofold: first, to investigate proposed models for the subgrid-scale variance and filtered dissipation rate (the "sub-models"), and second, to test LELFM with an accurate simulation of chemical reactions occurring in the laboratory flow of Comte-Bellot and Corrsin [6]. Although the theory is more general, this simplified case of an incompressible flow and a reaction without heat release is addressed in order to isolate the effects of the sub-models, and to eliminate questions about the physical correctness of the underlying velocity field, and thus the mixing process, in the simulations.

2. Subgrid-Scale Chemistry Model

2.1. Reaction zone physics

The LELFM formulation developed by Cook et al. [10] and Cook and Riley [9] is summarized below. All variables are nondimensional (for details about the nondimensionalization, see [9]). Consider a two-feed combustion problem with fuel carried by feed l and air carried by feed 2. As the fuel and air are mixed, chemical reactions occur, forming various combustion products. The mass fractions of the chemical species are denoted as Y_i and the reaction rates are denoted as $\dot{w}_i$. A mixture-fraction $\xi(\mathbf{x}, t)$ is defined, as in Bilger [1], so that, with the assumption of equal diffusivities of all species, ξ is a conserved scalar in the flow, having a value of unity in feed 1 and a value of zero in feed 2.

In typical combustion problems the zones of reaction are too small to be resolved by the LES; therefore, the chemistry must be modeled in its entirety. In deriving a model for the subgrid-scale chemistry, it is useful to note that the universal nature of the mixing of ξ at the small scales of turbulence is well documented, supported by detailed laboratory experimental evidence, data from DNS, and local solutions of the Navier–Stokes and scalar transport equations [3, 35, 39, 41]. This motivates the use of flamelet theory in formulating a subgrid-scale model for Y_i and w_i.

Peters [32] proposed the following set of equations, derived from the species conservation equations, as a means of relating the species mass fractions Y_i to the mixture-fraction ξ. These equations are expected to hold at high Damköhler numbers. (Note that the definition of χ employed here differs by a factor of $1/(2\rho)$, where ρ is the density, from that of Peters.)

$$-\chi \frac{\mathrm{d}^2 Y_i}{\mathrm{d}\xi^2} = \dot{w}_i, \quad i = 1, \ldots, N, \tag{1}$$

where N is the total number of chemical species in the flow and χ is the scalar dissipation rate, defined as

$$\chi = \frac{\mu}{\mathrm{Pe}} \nabla\xi \cdot \nabla\xi.$$

Here Pe is the Peclet number and μ is the dynamic viscosity, which accounts for possible temperature dependence of viscosity and molecular diffusivity. The equation set is coupled through the reaction rates, i.e., the $\dot{w}_i$ terms, which are functions of Y_i, ρ and temperature T. Equation (1) satisfies the boundary conditions:

$$Y_i(\xi = 0) = Y_{i2}, \tag{2}$$

$$Y_i(\xi = 1) = Y_{i1}, \tag{3}$$

where Y_{i1} and Y_{i2} are the uniform values of Y_i in feeds 1 and 2, respectively.

The dynamics of the local strain-diffusion competition involved in scalar mixing suggests that χ must be concentrated in locally one-dimensional, layer-like structures [3, 32]. The ξ dependence of χ is therefore prescribed as the solution to a one-dimensional, counterflow problem. The result is

$$\chi = \chi_o F(\xi), \tag{4}$$

where

$$F(\xi) = \exp\{-2[\mathrm{erf}^{-1}(2\xi)]^2\}.$$

Here χ_o is the local peak value of χ within the reaction layer, and erf^{-1} is the inverse error function (not the reciprocal).

2.2. Additional assumptions

In many devices, such as industrial gas furnaces, the combustion occurs at flow speeds much slower than the local speed of sound. The Mach number of these flows is low, yet the density varies due to heat release. In simulating these flows, the acoustic modes can be removed from the governing equations, resulting in significant computational savings. If a low Mach number approximation is applied to the governing equations, then the ideal gas equation becomes [26]

$$p^{(0)} = \rho T, \tag{5}$$

where $p^{(0)}$ is the first-order or thermodynamic pressure, which is uniform in space. If combustion takes place in an open domain, then $p^{(0)}$ is also constant in time, in which case ρ is known in terms of T alone. In such a regime, the number of parameters in Equation (1) can be reduced by relating T, and thereby ρ, to ξ and Y_i [22]. This is accomplished by using the total enthalpy, defined as

$$H = \frac{\gamma}{(\gamma - 1)} T + \sum_{i=1}^{N} h_i Y_i, \tag{6}$$

where γ is the ratio of specific heats and h_i are the enthalpies of formation of the various species. If the Prandtl number of the flow is equal to the Schmidt number, then the transport equations for H and ξ are identical. In such case, H is linearly related to ξ, the relationship given by

$$\begin{aligned} H &= \left[\frac{\gamma}{(\gamma - 1)} (T_1 - T_2) + \sum_{i=1}^{N} h_i (Y_{i1} - Y_{i2}) \right] \xi \\ &\quad + \frac{\gamma}{(\gamma - 1)} T_2 + \sum_{i=1}^{N} h_i Y_{i2}, \end{aligned} \tag{7}$$

where T_1 and T_2 are the temperatures in feeds 1 and 2 respectively. Using Equations (6) and (7), T can be expressed as a function of Y_i and ξ, i.e.,

$$\begin{aligned} T &= \left[T_1 - T_2 + \frac{(\gamma - 1)}{\gamma} \sum_{i=1}^{N} h_i (Y_{i1} - Y_{i2}) \right] \xi \\ &\quad + T_2 + \frac{(\gamma - 1)}{\gamma} \sum_{i=1}^{N} h_i (Y_{i2} - Y_i). \end{aligned} \tag{8}$$

With ρ and T known in terms of ξ and Y_i, Equation (4) is inserted into Equation (1) and the system, Equations (1), (2) and (3), is solved to obtain $Y_i(\xi, \chi_o)$. With the species mass fractions known in terms of ξ and χ_o, the reaction rates, i.e., $\dot{w}_i(\xi, \chi_o)$, can also be computed.

2.3. SUBGRID-SCALE PDF

By assuming that reactions occur in thin regions of one-dimensional counterflow, the ξ dependence of χ is known through Equation (4). In the modeling, it is assumed that χ_o is independent of ξ; therefore, the average value of Y_i within an LES grid cell can be expressed as

$$\overline{Y_i} = \int_0^1 \int_{\chi_o^-}^{\chi_o^+} Y_i(\xi, \chi_o) P(\chi_o) P(\xi)\, \mathrm{d}\chi_o\, \mathrm{d}\xi, \tag{9}$$

where χ_o^- and χ_o^+ are the minimum and maximum values of χ_o within the grid cell. The overbar denotes a spatially filtered scalar quantity defined by the convolution integral of the scalar with a normalized filter kernel function. In Equation (9), $P(\xi)$ is the LEPDF, giving the subgrid-scale probability density distribution of ξ within the cell. Likewise, $P(\chi_o)$ gives the subgrid-scale probability density of χ_o. To simplify notation, no distinction is made between the random variables and their probability space counterparts. Since the deviation between Y_i and its equilibrium limit depends weakly on χ_o [4, 16, 20], it follows that

$$\overline{Y_i} = \int_0^1 Y_i(\xi, \overline{\chi_o}) P(\xi)\, \mathrm{d}\xi. \tag{10}$$

The integral in Equation (10) is carried out by assuming a Beta distribution for $P(\xi)$. Williams [43] gives this distribution as

$$P(\xi) = \frac{\xi^{a-1}(1-\xi)^{b-1}}{B(a,b)}, \tag{11}$$

where

$$a = \overline{\xi}\left[\frac{\overline{\xi}(1-\overline{\xi})}{\xi_v^2} - 1\right], \quad b = a/\overline{\xi} - a, \quad \xi_v^2 = \overline{\xi^2} - \overline{\xi}^2.$$

In Equation (11) $B(a,b)$ is the Beta function and ξ_v^2 is the subgrid-scale variance of ξ. Finally, $\overline{\chi_o}$ is related to $\overline{\chi}$ by filtering (4), i.e.,

$$\overline{\chi} = \overline{\chi_o} \int_0^1 F(\xi) P(\xi)\, \mathrm{d}\xi. \tag{12}$$

2.4. CONSTRUCTING TABLES

In simulating variable density flows, it is common to work with Favre-filtered quantities. A Favre-filtered, i.e., density-weighted, variable is defined as

$$\widetilde{\phi} = \frac{\overline{\rho\phi}}{\overline{\rho}}, \tag{13}$$

and denoted by a tilde. The chemistry model may be employed in an LES by constructing tables for $\overline{Y_i}(\widetilde{\xi}, \widetilde{\xi^2}, \overline{\chi})$ and $\overline{\dot{w}_i}(\widetilde{\xi}, \widetilde{\xi^2}, \overline{\chi})$. The tables will depend on the flow parameters: $p^{(0)}$, T_1, T_2, h_i, Y_{i1}, Y_{i2}, Re, Sc, the various activation temperatures T_{ai}, and the various Damköhler numbers Da_i. The tables are constructed in the following way. First, $\overline{\xi}$ and $\overline{\xi^2}$ are chosen and $P(\xi)$ is determined from Equation (11). Then $\overline{\chi_o}$ is chosen and $\overline{\chi}$ is computed using Equation (12). The flamelet model solutions can then be computed and specified in terms of $Y_i(\xi, \overline{\chi})$. Next, Equation (8) is used, along with Equation (5) and $Y_i(\xi, \overline{\chi})$, to compute $\rho(\xi, \overline{\chi})$. With $P(\xi)$ and $\rho(\xi, \overline{\chi})$ known, $\widetilde{\xi}$ and $\widetilde{\xi^2}$ can then be computed. Finally, $\overline{Y_i}$ is computed from Equation (10) and $\overline{\dot{w}_i}$ is obtained similarly. Note that $\overline{Y_i}$ and $\overline{\dot{w}_i}$ are initially obtained in terms of $\overline{\xi}$, $\overline{\xi^2}$ and $\overline{\chi_o}$, but may be tabulated as functions of $\widetilde{\xi}$, $\widetilde{\xi^2}$ and $\overline{\chi}$. Also, since ρ is a known function of ξ and $\overline{\chi}$, the Favre-filtered variables $\widetilde{Y_i}$ and $\widetilde{\dot{w}_i}$ can also be computed and tabulated.

2.5. Obtaining $\widetilde{\xi}$ and $\widetilde{\xi^2}$

The tables for $\overline{Y_i}$ and $\overline{\dot{w}_i}$ require $\widetilde{\xi}$, $\widetilde{\xi^2}$ and $\overline{\chi}$ as inputs. Therefore, these quantities must be obtained in addition to the velocity field and other LES variables. In an LES, $\widetilde{\xi}$ is computed by integrating its transport equation. The transport equation for ξ is

$$\frac{\partial \rho\xi}{\partial t} + \frac{\partial \rho\xi u_j}{\partial x_j} = \frac{1}{\mathrm{Pe}} \frac{\partial}{\partial x_j}\left(\mu \frac{\partial \xi}{\partial x_j}\right). \tag{14}$$

An equation for $\widetilde{\xi}$ is derived by Favre-filtering Equation (14) and neglecting the term due to subgrid fluctuations in μ; this gives

$$\frac{\partial \overline{\rho}\widetilde{\xi}}{\partial t} + \frac{\partial \overline{\rho}\widetilde{\xi}\widetilde{u}_j}{\partial x_j} = \frac{1}{\mathrm{Pe}} \frac{\partial}{\partial x_j}\left(\overline{\mu} \frac{\partial \widetilde{\xi}}{\partial x_j}\right) - \frac{\partial \zeta_j}{\partial x_j}, \tag{15}$$

where $\zeta_j \equiv \overline{\rho}(\widetilde{u_j\xi} - \widetilde{u}_j\widetilde{\xi})$ must be modeled.

There are several ways of obtaining $\widetilde{\xi^2}$, one of which is to integrate its governing equation [37], which is obtained by multiplying Equation (14) by ξ and Favre-filtering (again ignoring subgrid fluctuations in the diffusivity). The result is

$$\frac{\partial \overline{\rho}\widetilde{\xi^2}}{\partial t} + \frac{\partial \overline{\rho}\widetilde{u}_j\widetilde{\xi^2}}{\partial x_j} = \frac{1}{\mathrm{Pe}} \frac{\partial}{\partial x_j}\left(\overline{\mu} \frac{\partial \widetilde{\xi^2}}{\partial x_j}\right) - 2\overline{\chi} - \frac{\partial \eta_j}{\partial x_j}, \tag{16}$$

where $\eta_j \equiv \overline{\rho}(\widetilde{u_j\xi^2} - \widetilde{u}_j\widetilde{\xi^2})$ must also be modeled. One difficulty with this method is in developing the initial $\widetilde{\xi^2}$ field. Another way to determine $\widetilde{\xi^2}$ is via a model which relates it to the magnitude of the gradient of $\widetilde{\xi}$, i.e.,

$$\widetilde{\xi^2} = \widetilde{\xi}^2 + C_\xi \overline{\rho} \Delta^2 \nabla\widetilde{\xi} \cdot \nabla\widetilde{\xi}, \tag{17}$$

where the C_ξ can be computed dynamically [7, 24, 44]. Here Δ is the characteristic width of the "grid" filter, i.e., the Favre filter which is applied to remove scales too small to be resolved on the LES numerical grid.

In this work, $\widetilde{\xi^2}$ is computed in terms of the SGS variance, ξ_v^2, by assuming similarity between the subgrid-scales and the smallest resolved scales, as proposed by Cook and Riley [8]. Such a model was tested by Jiménez et al. [19] and was successfully used by Réveillon and Vervisch [34] in an LES of reacting turbulence. For the general case of variable-density turbulence, a SGS "Favre variance" is defined as follows

$$\xi_f^2 \equiv (\widetilde{\xi^2} - \widetilde{\xi}^2) = \left(\overline{\rho\xi^2} - \overline{\rho\xi}^2 \Big/ \overline{\rho}\right) \Big/ \overline{\rho}. \tag{18}$$

A "test" filter, with a characteristic width greater than that of the grid filter, is then defined and denoted by a $\widehat{(\,)}$. A test filter-scale variance is defined by analogy to Equation (18), i.e.,

$$Z_f^2 \equiv \left(\widehat{\overline{\rho\xi^2}} - \widehat{\overline{\rho\xi}}^2 \Big/ \widehat{\overline{\rho}}\right) \Big/ \overline{\rho}. \tag{19}$$

The model for ξ_f^2 assumes scale similarity between ξ_f^2 and $Z_f^2 - \widehat{\xi_f^2}$, and is denoted ξ_m^2, i.e.,

$$\xi_f^2 \approx \xi_m^2 \equiv c_L \left(\widehat{\overline{\rho}\widetilde{\xi^2}} - \widehat{\overline{\rho}\widetilde{\xi}}^2 \Big/ \widehat{\overline{\rho}}\right). \tag{20}$$

The above derivation is similar to the one by Moin et al. [28] for compressible flow. For low Mach number combustion in which ρ is a known function of ξ and the species mass fractions, the mean square, $\overline{\xi^2}$, (needed by the assumed beta PDF) can be related to the Favre variance, ξ_f^2, using the assumed beta PDF.

The quantity c_L is computed by assuming a form for the unresolved portion of the scalar energy spectrum. In an LES at high Reynolds number, the inertial range will extend to wavenumbers which make an insignificant contribution to the SGS variance. If the grid filter is in the inertial range, it is reasonable to assume $E_\xi(k) \propto k^{-5/3}$ for all SGS k, and to ignore details of the spectrum in the dissipation range. Here k is the magnitude of the three-dimensional wave number vector. In moderate Reynolds number flows, such as those examined in Section 3 of this paper, the dissipation range accounts for a significant amount of the SGS variance and cannot be ignored. Therefore, a form for the high wavenumber spectrum derived by Pao [31] is used:

$$E_\xi(k) \propto k^{-5/3} \exp(-0.89 D \varepsilon_T^{-1/3} k^{4/3}). \tag{21}$$

The only parameter, ε_T, is the kinetic energy transfered out of the resolved scales, a quantity which is known in an LES. The constant of proportionality is determined by matching the assumed spectrum to the known spectrum at the highest resolved wavenumber.

2.6. A MODEL FOR $\overline{\chi}$

In order to develop a model for $\overline{\chi}$, consider the equation for $\widetilde{\xi}$-energy, obtained by multiplying Equation (15) by $\widetilde{\xi}$, which, after some algebra, gives

$$\frac{\partial \overline{\rho}\widetilde{\xi}^2}{\partial t} + \frac{\partial \overline{\rho}\widetilde{\xi}^2\widetilde{u}_j}{\partial x_j} = \frac{1}{\mathrm{Pe}}\frac{\partial}{\partial x_j}\left(\overline{\mu}\frac{\partial \widetilde{\xi}^2}{\partial x_j}\right) - 2\frac{\overline{\mu}}{\mathrm{Pe}}\left(\frac{\partial \widetilde{\xi}}{\partial x_j}\right)^2 - 2\widetilde{\xi}\frac{\partial \zeta_j}{\partial x_j}, \tag{22}$$

where ζ_j is defined above. We model ζ_i in a manner similar to Smagorinsky [40], i.e.,

$$\zeta_i = -\frac{\mu_t}{\mathrm{Sc}_t}\frac{\partial \widetilde{\xi}}{\partial x_i}, \tag{23}$$

where Sc_t is a subgrid-scale Schmidt number, assumed to be unity in this work, and the subgrid-scale viscosity is defined as

$$\mu_t = C_{\mathbf{x},t}\overline{\rho}\Delta^2\left|\widetilde{S}\right|. \tag{24}$$

Here, $C_{\mathbf{x},t}$ is a dynamically determined coefficient [15], $\left|\widetilde{S}\right|$ is the magnitude of the resolved strain-rate tensor, and Δ is the characteristic width of the LES grid filter.

Inserting Equation (23) into Equation (22) yields

$$\begin{aligned}\frac{\partial \overline{\rho}\widetilde{\xi}^2}{\partial t} + \frac{\partial \overline{\rho}\widetilde{\xi}^2\widetilde{u}_j}{\partial x_j} &= \frac{2}{\mathrm{Pe}}\frac{\partial}{\partial x_j}\left(\widetilde{\xi}\overline{\mu}\frac{\partial \widetilde{\xi}}{\partial x_j}\right) \\ &+ \frac{1}{\mathrm{Sc}_{sgs}}\frac{\partial}{\partial x_j}\left(\mu_t\frac{\partial \widetilde{\xi}^2}{\partial x_j}\right) - \frac{2\overline{\mu}}{\mathrm{Pe}}\left(\frac{\partial \widetilde{\xi}}{\partial x_j}\right)^2 - \frac{2\mu_t}{\mathrm{Sc}_t}\left(\frac{\partial \widetilde{\xi}}{\partial x_j}\right)^2.\end{aligned} \tag{25}$$

The last two terms represent the dissipation rate of $\widetilde{\xi}$ due to molecular effects and the transfer of $\widetilde{\xi}$ energy to the subgrid-scales, respectively.

We note that, at the larger scales, $\widetilde{\xi}^2$ is approximately equal to $\widetilde{\xi}^2$, the difference between the two being due to the filtering of ξ at the smaller scales. This implies, in particular, that the spectral transfer rate of both quantities to the subgrid scales is nearly identical. Assuming in addition that the transfer rate of $\widetilde{\xi}$ to the subgrid scales is equal to its dissipation rate at those scales, a comparison of Equations (16) and (25) suggests the model for $\overline{\chi}$:

$$\overline{\chi}_m \equiv \left(\frac{\overline{\mu}}{\mathrm{Pe}} + \frac{\mu_t}{\mathrm{Sc}_t}\right)\left(\frac{\partial \widetilde{\xi}}{\partial x_j}\right)^2. \tag{26}$$

This is the first term in a model for $\overline{\chi}$ proposed by Girimaji and Zhou [17]. We will take Equation (26) as our model for $\overline{\chi}$.

3. Results

Data sets from Direct Numerical Simulations of an isothermal, one-step chemical reaction were used to investigate the accuracy of the LELFM and the sub-models.

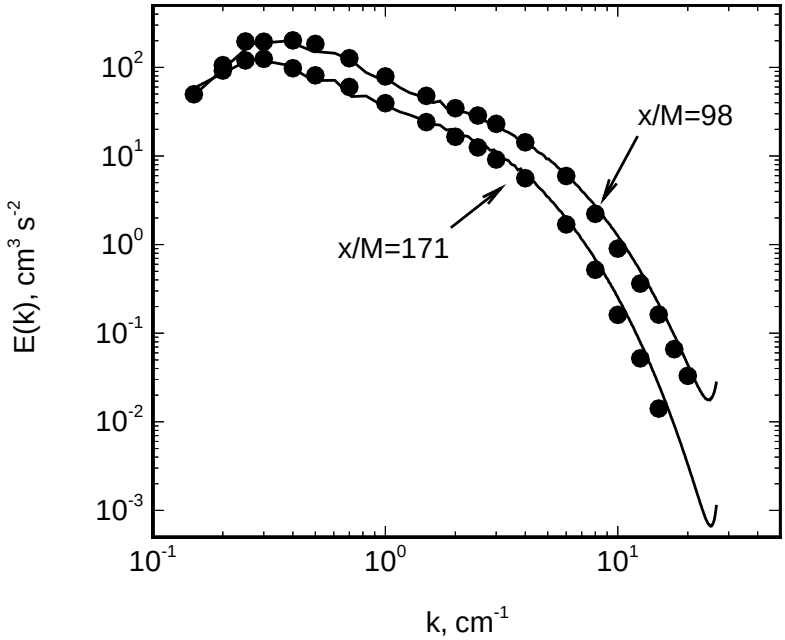

Figure 1. Three dimensional kinetic energy spectra. The symbols are laboratory data [6], the lines are from the DNS.

The model formulation in Section 2 applies to the general problem of multi-step reactions with heat release, but the simplified case is examined here as a first test of the sub-models. The velocity field is that of the laboratory experiment of Comte-Bellot and Corrsin [6] in which nearly isotropic, incompressible turbulence decays downstream of a grid of spacing M oriented normal to a uniform, steady flow. Statistical data were collected in the laboratory at downstream locations $x/M = 42$, 98, and 171. The Reynolds number at the first station, based on the Taylor length scale and the rms velocity, is 71.6. The numerical simulations are performed with a pseudo-spectral code using a 512^3-point periodic domain considered to be moving with the mean flow, and are in dimensional units (centimeters and seconds) with no scaling between the laboratory and simulation parameters. Taylor's hypothesis is invoked to relate simulated time to laboratory coordinates. The simulation velocity field is initialized to match the laboratory kinetic energy spectrum at $x/M = 42$. In the computer code, Fourier pseudo-spectral methods are used to approximate spatial derivatives, and a second-order Adams–Bashforth scheme with pressure-projection is used for time-stepping. Figure 1 shows that the three-dimensional kinetic energy spectra for the DNS at later times are almost identical to that of the corresponding spectra from the laboratory flow; this gives confidence that the scalar mixing in the numerical experiment should be very similar to that which would occur in a physical flow. For additional details on the accuracy of the DNS velocity field, see [11].

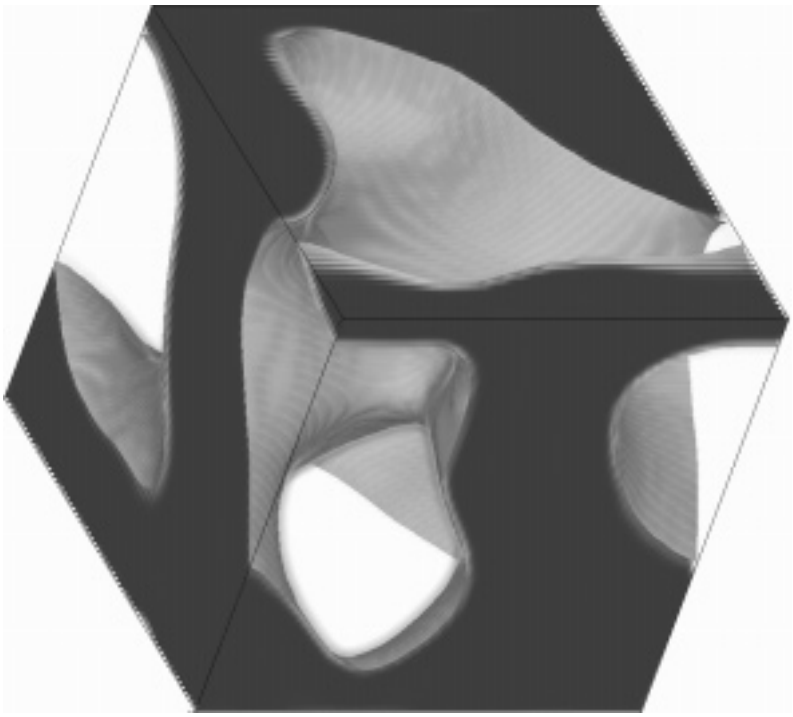

Figure 2. The initial scalar field. The dark area is fuel.

The initial ξ field is similar to the "large blob" case of Mell et al. [27] (also used by Nilsen and Kosály [29, 30]). In those studies, the computational domain was smaller, relative to the integral length scale of the velocity field, than in the present simulations, and that the ratio of the velocity and scalar integral length scales was about unity. For the simulations reported here, the ξ-field was scaled to fill the larger computational domain so that the ratio of the scalar and velocity integral length scales is about three. The scalar field is a contorted blob in which $\xi = 1$ occupies about half of the computational domain, and $\xi = 0$ in the remainder of the domain; Figure 2 is a three-dimensional rendering of the field. This scalar field evolves with the velocity field beginning at $x/M = 42$. At $x/M = 98$, the fuel field, Y_f, is initialized from ξ by using the flamelet model of Peters [32], at which point the following reaction develops:

$$\text{Fuel} + \text{Oxidizer} \rightarrow \text{Product}. \tag{27}$$

The reaction rate constant, $A = -\dot{w_f}/(Y_f Y_o)$, is 30, so that the initial ratio of the mixing and chemical timescales, Al/u, is approximately the same as it is in the fast chemistry cases of Mell et al. [27] and Nilsen and Kosály [30]. Here, l is the integral length scale of the velocity field and u is the rms velocity at $x/M = 98$.

In order to test the LELFM and the sub-models, the DNS data fields are filtered onto a $32 \times 32 \times 32$ point LES mesh using a top-hat filter. Then "exact" values for

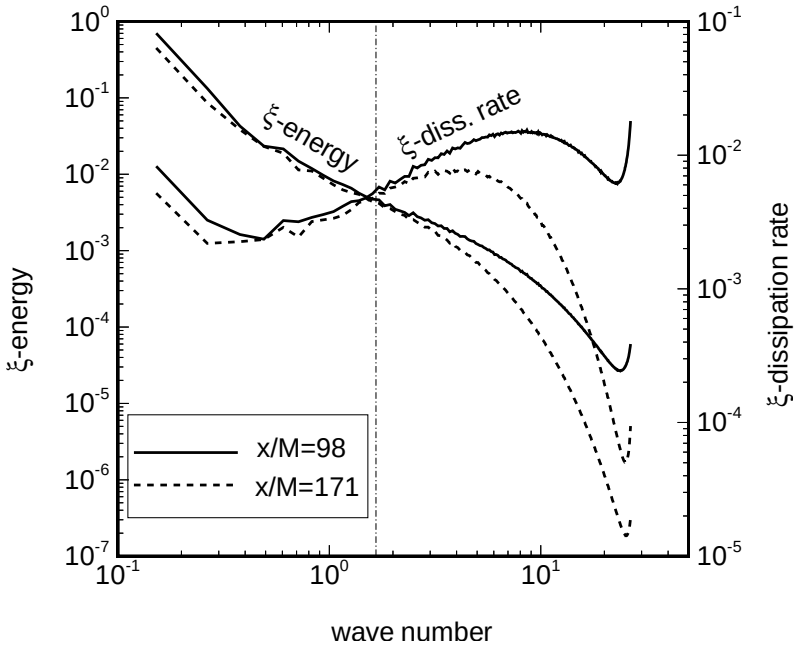

Figure 3. Scalar energy and dissipation rate spectra from the DNS. The vertical dash-dot line indicates the maximum wave number in the 32^3 LES fields.

$\overline{Y_p}$, $\overline{\xi}$, ξ_v^2, and $\overline{\chi}$ are computed by averaging over the $(32)^3$ DNS grid points in each LES grid cell. The latter two quantities are taken to be the exact sub-model values, which are denoted $\overline{\chi}_e$ and ξ_e^2. Since the intent of LES is to resolve the large eddies, the filtered DNS fields represent an LES only if they contain the majority of the energy containing scales, but do not contain the scales that account for the bulk of the energy dissipation rate. This is demonstrated to be the case in Figure 3, which shows the scalar energy and dissipation rate spectra at $x/M = 98$ and $x/M = 171$. Filtering the DNS fields to $16 \times 16 \times 16$ would further eliminate the scales responsible for energy dissipation, but would not leave enough grid points from which to compute ξ_m^2, since this calculation requires the application of the coarser test filter.

3.1. EVALUATION OF THE MODEL FOR $\overline{\chi}$

To evaluate $\overline{\chi}_m$, we conduct an *a priori* pointwise comparison of $\overline{\chi}$ and $\overline{\chi}_m$ using DNS data, and then examine the effect that the error in $\overline{\chi}_m$ has on the LELFM predictions of the spatially averaged filtered product mass fraction, $\langle \overline{Y_p} \rangle$. In the *a priori* tests, two correlations are of interest: the first is between $\overline{\chi}$ and the filtered square of the resolved-scale scalar gradient, $\overline{\nabla\overline{\xi} \cdot \nabla\overline{\xi}}$. The correlation coefficient for these two quantities ranges from 0.84 at $x/M = 98$ to 0.79 at $x/M = 171$, which supports the concept of relating $\overline{\chi}_m$ to $\overline{\nabla\overline{\xi} \cdot \nabla\overline{\xi}}$. The correlation coefficient

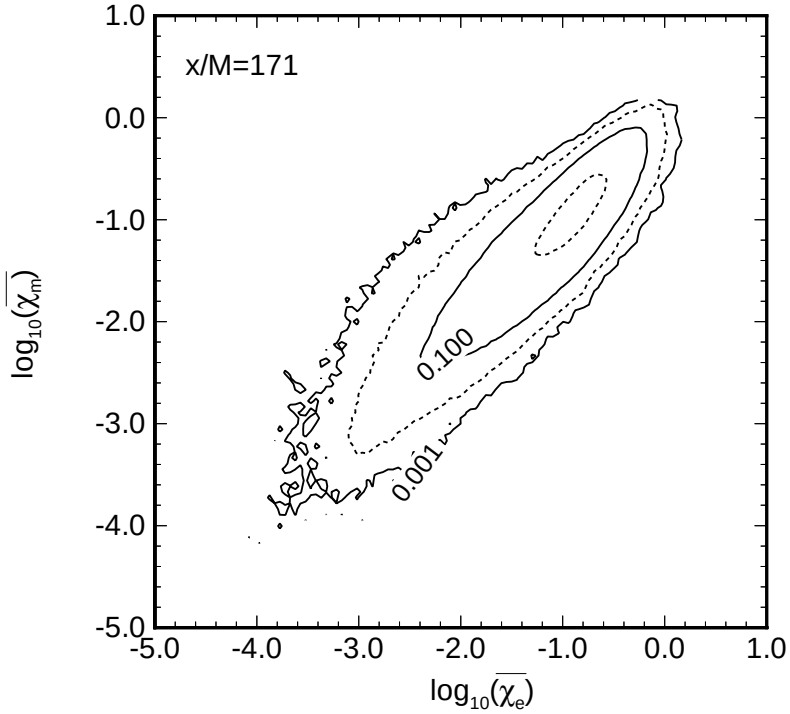

Figure 4. Joint PDF of exact and modeled filtered dissipation rate for 32^3 simulated LES. Contour lines are logarithmically spaced.

between $\overline{\chi}$ and $\overline{\chi}_m$ ranges from 0.74 to 0.76 indicating that the use of the coefficient $((\overline{\mu}/\mathrm{Pe}) + (\mu_t/\mathrm{Sc}_t))$ in Equation (26) introduces some scatter between $\overline{\chi}$ and $\overline{\chi}_m$. On average, $\overline{\chi}_m$ is 20–25% of $\overline{\chi}$ for the 32^3 resolution discussed in this work, but the percentage increases to 45% when the DNS data is filtered onto a 64^3 mesh. The joint PDF of $\overline{\chi}_e$ and $\overline{\chi}_m$ at $x/M = 171$ is shown in Figure 4.

The second phase of the testing of the model for $\overline{\chi}$ is to compare LELFM predictions of $\langle \overline{Y_p} \rangle$ using the exact value of $\overline{\chi}$ from DNS, $\overline{\chi}_e$, and using the modeled value, $\overline{\chi}_m$. Figure 5 shows the predictions as a function of x/M, along with the DNS results. The curve on the plot denoted e is computed using $\overline{\chi}_e$ and ξ_e^2, while the curve denoted m is computed with $\overline{\chi}_m$ and ξ_e^2. Thus, the difference between the two curves is due to the error in $\overline{\chi}_m$; not only is this difference small, the ratio between the curves is much closer to unity than the ratio of $\overline{\chi}_m$ to $\overline{\chi}$, i.e., the chemistry model is only weakly influenced by errors in the filtered scalar dissipation rate. There are two reasons for this. First, the error in $\overline{\chi}_m$ is very small for the majority of points in the field. Second, the filtered product mass fraction is only weakly sensitive to $\overline{\chi}$, so that the chemical concentrations will not be very sensitive to errors in $\overline{\chi}_m$. This last point is demonstrated in Figure 6, which shows the filtered product mass fraction predicted by LELFM at the stoichiometric surface as a function of ξ_v^2 and the local filtered Damköhler number, $\overline{\mathrm{Da}} \propto A/\overline{\chi}$.

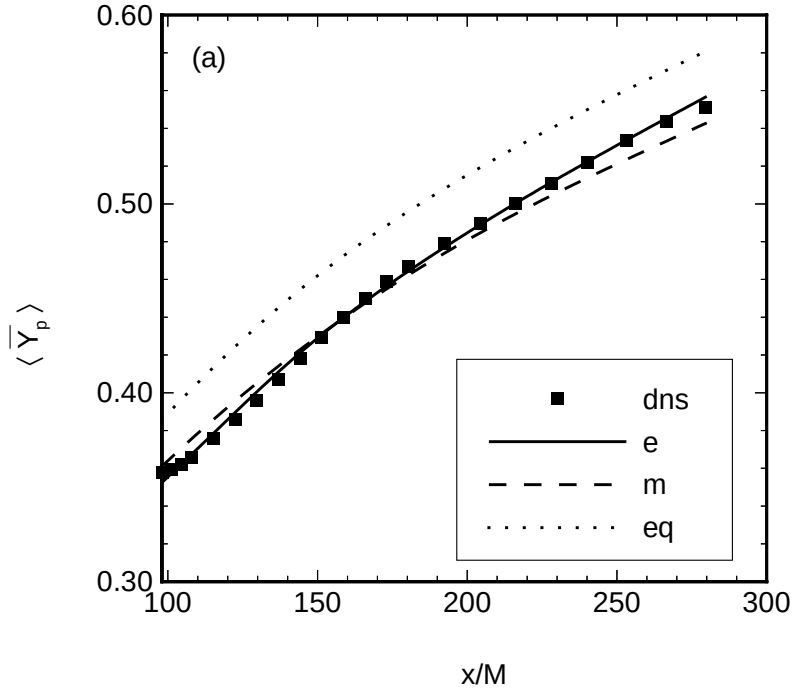

Figure 5. Mean product from DNS and as predicted by LELFM. e: $\overline{\chi}_e$ and ξ_e^2 were used in place of the sub-models. m: $\overline{\chi}_m$ and ξ_e^2 were used. The curve using $\overline{\chi}_m$ and ξ_m^2 nearly coincides with m and is not shown. eq denotes the equilibrium chemistry limit.

In this work, $10^0 < \overline{\mathrm{Da}} < 10^4$ for most of the points in the filtered DNS fields. The figure shows the low sensitivity of $\overline{Y_p}$ to a change in $\overline{\mathrm{Da}}$ when $\xi_v^2 = 0$, and that this sensitivity decreases further as ξ_v^2 increases. A half decade change in $\overline{\mathrm{Da}}$ corresponds to at most a 10% change $\overline{Y_p}$. It is also important to note from the figure that an underprediction of $\overline{\chi}$ ($\overline{\mathrm{Da}}$ too high) causes the computed value of $\overline{Y_p}$ to be too high, and an underprediction of ξ_v^2 has the same effect.

3.2. Evaluation of the model for ξ_v^2

A similar analysis can be carried out for the ξ_v^2 model as was done for the $\overline{\chi}$ model. The correlation between ξ_e^2 and ξ_m^2 decreases slowly with downstream distance from 0.87 at $x/M = 98$ to 0.82 at $x/M = 171$. On average, ξ_m^2 underpredicts ξ_e^2 by about 7% because the assumed shape of the ξ-energy spectrum (21) does not exactly match the true spectrum; however the effect of the error in ξ_m^2 on $\langle \overline{Y_p} \rangle$ is negligible. The joint PDF of ξ_e^2 and ξ_m^2 at $x/M = 171$ is shown in Figure 7. The contour lines on the plot are logarithmically spaced, which means that a small fraction of the subgrid-scale volumes are responsible for most of the scatter; for the majority of the points, the model is very accurate. Also, even at this late time,

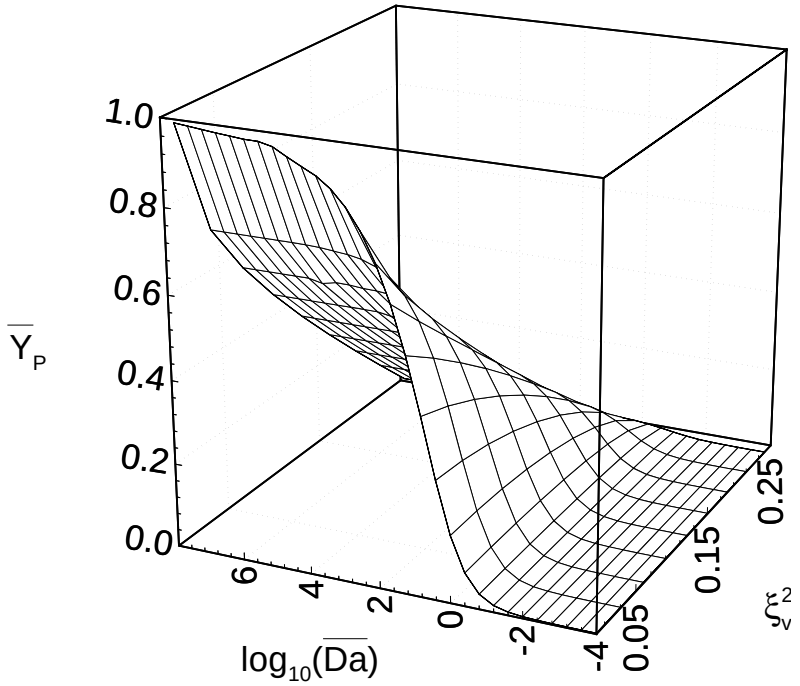

Figure 6. Equation (10) evaluated for product at the stoichiometric surface.

when considerable mixing and reaction have occurred, the subgrid-scale variance in most points is quite low.

3.3. EVALUATION OF THE OVERALL MODEL

The true test of the LELFM is accomplished by examining predictions of local filtered species mass fractions and the same quantity spatially averaged. Figure 5 shows that the spatially averaged predictions are very good compared with the DNS results at all downstream locations. The symbols represent the filtered DNS results and the line marked "eq" is the equilibrium chemistry limit based on the mixture fraction from the DNS. The line marked "e" represents the LELFM predictions when $\overline{\chi}$ and ξ_v^2 are taken from the DNS; for the reaction rate used in this work, the predictions nearly coincide with the DNS data over the full range of x/M. The line marked "m" represents the LELFM predictions when ξ_v^2 is taken from the DNS and $\overline{\chi}$ is modeled by $\overline{\chi}_m$, so that differences between the "m" and "e" lines are due to errors in $\overline{\chi}_m$. Errors introduced into the LELFM predictions by ξ_m^2 are insignificant and are not shown.

To examine the local behavior of the predictions for $\overline{Y_p}$, the joint probability density of the LELFM predictions (using both sub-models) and the filtered DNS results are displayed in Figure 8 for $x/M = 171$. Again, the contour lines are logarithmically spaced and the model is seen to be quite accurate at most locations.

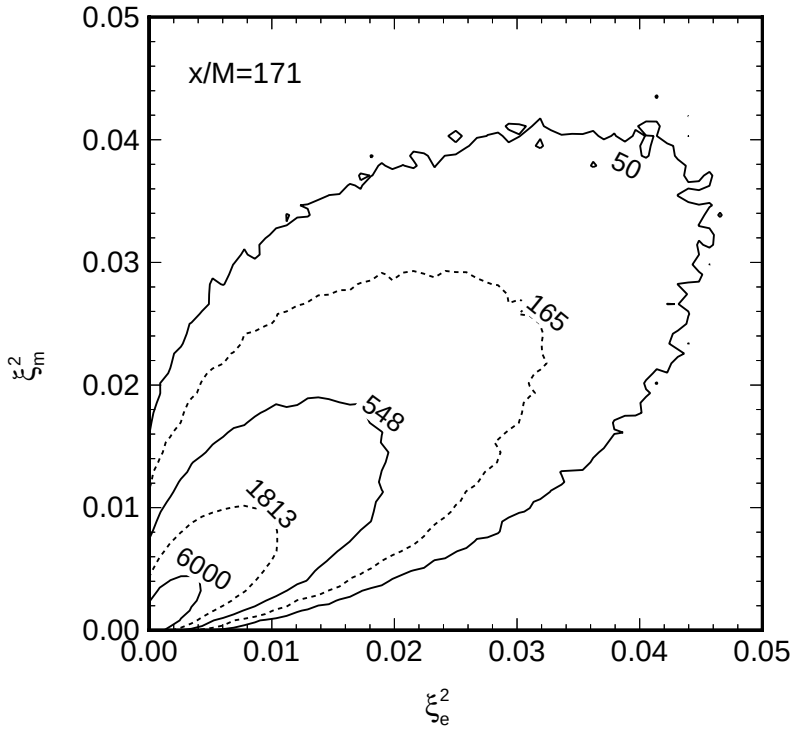

Figure 7. Joint PDF of ξ_e^2 and ξ_m^2. The contour lines are logarithmically spaced.

The correlation between the exact $\overline{Y_p}$ and the LELFM prediction (using $\overline{\chi}_m$ and ξ_m^2) is 0.96, and the slope of the least squares fit of the data is 1.1. At this downstream location, there are regions where little mixing has occurred, and others where considerable mixing and reaction have taken place, resulting in filtered product mass fractions ranging from 0 to about 0.7; from Figure 8 it is evident that the overall subgrid-scale chemistry model accurately predicts the product over the range of conditions, but is biased toward slightly overpredicting $\overline{Y}_p$, especially when the exact $\overline{Y}_p$ is high.

4. Conclusions

The LELFM has been previously demonstrated to accurately predict filtered chemical species $\overline{Y_i}$ and filtered reaction rates $\overline{\dot{w}_i}$ in *a priori* tests of turbulent reacting flows when the subgrid-scale scalar variance and its filtered dissipation rate are known exactly, given a large enough Damköhler number [9, 10]. This paper presents models for those two quantities, and demonstrates that LELFM continues to make very good predictions of the filtered product mass fraction in a one-step, isothermal reaction. The subgrid-scale variance predicted by the scale similarity model has high correlation with the exact values and, on average, the magnitude of

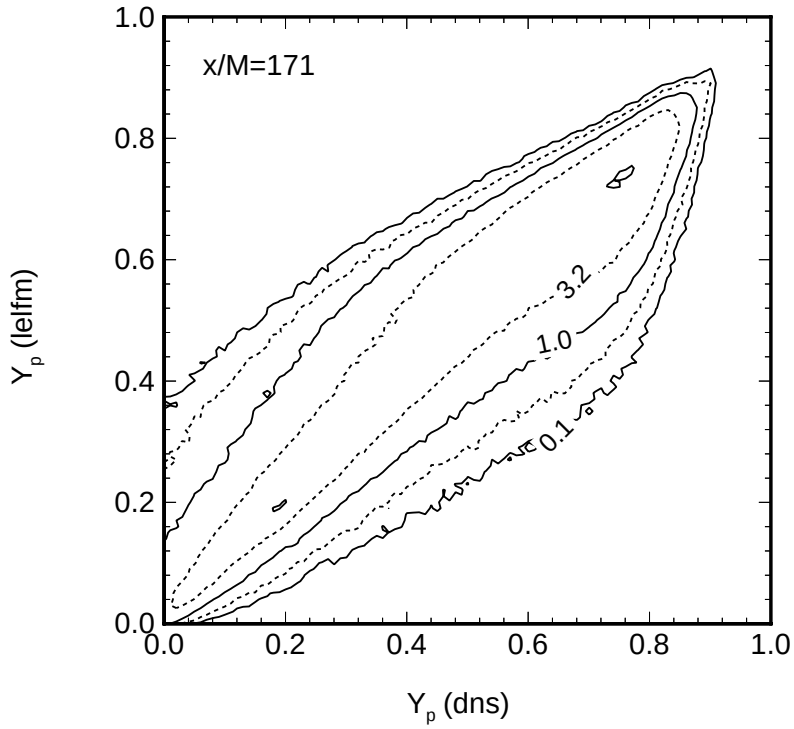

Figure 8. Joint PDF of the exact $\overline{Y}_p$ (from DNS) and the LELFM prediction of $\overline{Y}_p$. The LELFM calculation is done using $\overline{\chi}_m$ and ξ_m^2. The contour lines are logarithmically spaced.

the variance is predicted to within about 7% by assuming a form for the unresolved portion of the scalar energy spectrum. The effect of errors in the prediction of the variance on the LELFM prediction of filtered product is negligible. The filtered dissipation rate is computed from the magnitude of the resolved-scale scalar gradient and a subgrid-scale diffusivity; the correlation between the modeled and exact values is good and, on average, the magnitude of the modeled value is low. The effect of errors in the model for the dissipation rate on the LELFM predictions of the filtered product are small but discernible.

Acknowledgements

This work is supported by the National Science Foundation (grant No. CTS-9415280) and the Air Force Office of Scientific Research (grant No. 49620-97-1-0092), and by grants of high performance computing (HPC) time from the Arctic Region Supercomputing Center and the Pittsburgh Supercomputing Center.

References

1. Bilger, R.W., Turbulent flows with nonpremixed reactants. In Libby, P.A. and Williams, F.A. (eds), *Turbulent Reacting Flows*, Topics in Applied Physics, Vol. 44. Springer-Verlag, Berlin (1980) pp. 65–113.
2. Branley, N. and Jones, W.P., Large eddy simulation of a turbulent non-premixed flame. In: *Proceedings of the Eleventh Symposium on Turbulent Shear Flows*, Grenoble, France (1997) pp. 21.1–21.6.
3. Buch, K.A. and Dahm, W. J.A., Experimental-study of the fine-scale structure of conserved scalar mixing in turbulent shear flows. Part I: Sc $\gg$ 1. *J. Fluid Mech.* **317** (1996) 21–71.
4. Buriko, Y.Y., Kuznetsov, V.R., Volkov, D.V., Zaitsev, S.A. and Uryvsky, A.F., A test of a flamelet model for turbulent nonpremixed combustion. *Combust. Flame* **96** (1994) 104–120.
5. Colucci, P.J., Jaberi, F.A., Givi, P. and Pope, S.B., Filtered density function for large eddy simulation of turbulent reacting flows. *Phys. Fluids* **10** (1998) 499–515.
6. Comte-Bellot, G. and Corrsin, S., Simple Eulerian time correlation of full and narrow-band velocity signals in grid-generated, 'isotropic' turbulence. *J. Fluid Mech.* **48** (1971) 273–337.
7. Cook, A.W., On the simulation and modeling of turbulent reacting flows. Ph.D. Thesis. University of Washington, Seattle, WA (1996).
8. Cook, A.W. and Riley, J.J., A subgrid model for equilibrium chemistry in turbulent flows. *Phys. Fluids* **6** (1994) 2868–2870.
9. Cook, A.W. and Riley, J.J., Subgrid-scale modeling for turbulent, reacting flows. *Combust. Flame* **112** (1997) 593–606.
10. Cook, A.W., Riley, J.J. and Kosály, G., A laminar flamelet approach to subgrid-scale chemistry in turbulent flows. *Combust. Flame* **109** (1997) 332–341.
11. de Bruyn Kops, S.M. and Riley, J.J., Direct numerical simulation of laboratory experiments in isotropic turbulence. *Phys. Fluids* **10** (1998) 2125–2127.
12. Frankel, S.H., Adumitroaie, V., Madnia, C.K. and Givi, P., Large-eddy simulation of turbulent reacting flows by assumed PDF methods. In: *Engineering Applications of Large Eddy Simulations*. ASME, New York (1993) pp. 81–101.
13. Fureby, C., Lundgren, E. and Moller, S.I., Large-eddy simulations of bluff body stabilized flames. In: *25th Symposium (International) on Combustion*. Combustion Institute, Pittsburgh, PA (1994) pp. 1257–1264.
14. Gao, F. and O'Brien, E.E., A large-eddy simulation scheme for turbulent reacting flows. *Phys. Fluids A* **5** (1993) 1282–1284.
15. Germano, M., Piomelli, U., Moin, P. and Cabot, W.H., A dynamic subgrid-scale eddy viscosity model. *Phys. Fluids A* **3** (1991) 1760–1765.
16. Gibson, C.H. and Libby, P.A., On turbulent flows with fast chemical reactions. Part II. The distribution of reactants and products near a reaction surface. *Combust. Sci. Technol.* **6** (1972) 29–35.
17. Girimaji, S.S. and Zhou, Y., Analysis and modeling of subgrid scalar mixing using numerical data. *Phys. Fluids A* **8** (1996) 1224–1236.
18. Givi, P., Model free simulations of turbulent reactive flows. *Prog. Energy Combust. Sci.* **15** (1989) 1–107.
19. Jiménez, J., Liñán, A., Rogers, M.M. and Higuera, F.J., A-priori testing of sub-grid models for chemically reacting nonpremixed turbulent shear flows. *J. Fluid Mech.* **349** (1997) 149–171.
20. Kuznetsov, V.R. and Sabel'nikov, V.A., *Turbulence and Combustion*. Hemisphere, New York (1990).
21. Lentini, D., Assessment of the stretched laminar flamelet approach for non-premixed turbulent combustion. *Combust. Sci. Technol.* 100 (1994) 95–122.
22. Libby, P.A. and Williams, F.A., *Turbulent Reacting Flows*, Topics in Applied Physics, Vol. 44. Springer-Verlag, Berlin (1980).

23. Liou, T.M., Lien, W.Y. and Hwang, P.W., Large-eddy simulations of turbulent reacting flows in chamber with gaseous ethylene injecting through the porous wall. *Combust. Flame* **99** (1994) 591–600.
24. Mathey, F. and Chollet, J.P., Sub-grid model of scalar mixing for large eddy simulations of turbulent flows. In: *The Second ERCOFTAC Workshop on Direct and Large Eddy Simulations*, Grenoble, France (1996).
25. McMurtry, P.A., Menon, S. and Kerstein, A.R., A linear eddy sub-grid model for turbulent reacting flows: Application to hydrogen-air combustion. In: *Twenty-Fourth Symposium (International) on Combustion*. The Combustion Institute, Pittsburgh, PA (1992) pp. 271–278.
26. McMurtry, P.A., Riley, J.J. and Metcalfe, R.W., Effects of heat release on the large-scale structures in turbulent mixing layers. *J. Fluid Mech.* **199** (1989) 297–332.
27. Mell, W.E., Nilsen, V., Kosály, G. and Riley, J.J., Investigation of closure models for turbulent reacting flow. *Phys. Fluids A* **6** (1994) 1331–1356.
28. Moin, P., Squires, K., Cabot, W. and Lee, S., A dynamic subgrid-scale model for compressible turbulence and scalar transport. *Phys. Fluids A* **3** (1991) 2746–2757.
29. Nilsen, V. and Kosály, G., Differentially diffusing scalars in turbulence. *Phys. Fluids* **9** (1997) 3386–3397.
30. Nilsen, V. and Kosàly, G., Differential diffusion in turbulent reacting flows. *Combust. Flame* (accepted for publication).
31. Pao, Y.H., Structure of turbulent velocity and scalar fields at large wavenumbers. *Phys. Fluids* **8** (1965) 1063–1075.
32. Peters, N., Laminar diffusion flamelet models in non-premixed turbulent combustion. *Prog. Energy Combust. Sci.* **10** (1984) 319–339.
33. Pitsch, H., Chen, M. and Peters, N., Unsteady flamelet modeling of turbulent hydrogen/air diffusion flames. *27th International Symposium on Combustion*, Denver, CO (1998).
34. Réveillon, J. and Vervisch, L., Response of the dynamic LES model to heat release induced effects. *Phys. Fluids A* **8** (1996) 2248–2250.
35. Ruetsch, G.R. and Maxey, M.R., Small-scale features of vorticity and passive scalar fields in homogeneous isotropic turbulence. *Phys. Fluids A* **3** (1991) 1587–1597.
36. Sanders, J.P.H., Chen, J.Y. and Gökalp, I., Flamelet based modeling of NO formation in turbulent hydrogen jet diffusion flames. *Combust. Flame* **111** (1997) 1–15.
37. Schmidt, H. and Schumann, U., Coherent structure of the convective boundary layer derived from large-eddy simulations. *J. Fluid Mech.* **200** (1989) 511–562.
38. Schumann, U., Large eddy simulation of turbulent diffusion with chemical reactions in the convective boundary layer. *Atmos. Environ.* **23** (1989) 1713–1727.
39. Siggia, E.D., Numerical study of small-scale intermittency in three-dimensional turbulence. *J. Fluid Mech.* **107** (1981) 375–406.
40. Smagorinsky, J., General circulation experiments with the primitive equations. I. The basic experiment. *Mon. Weather Rev.* **91** (1963) 99–164.
41. Southerland, K.B. and Dahm, W.J.A., A four-dimensional experimental study of conserved scalar mixing in turbulent flows. Report No. 026779-12, The University of Michigan, Ann Arbor, MI (1994).
42. Sykes, R.I., Henn, D.S., Parker, S.F. and Lewellen, W.S., Large-eddy simulations of a turbulent reacting plume. *Atmos. Environ A* **26** (1992) 2565–2574.
43. Williams, F.A., *Combustion Theory: The Fundamental Theory of Chemically Reacting Flow Systems*. Benjamin-Cummings, Menlo Park, CA (1985).
44. Yoshizawa, A., Statistical theory for compressible turbulent shear flows, with the application to subgrid modeling. *Phys. Fluids A* **29** (1986) 2152–2164.